Journal of Catalysis 356 (2017) 173–185

Contents lists available at ScienceDirect

Journal of Catalysis

journal homepage: www.elsevier.com/locate/jcat

Synthesis of highly dispersed cobalt oxide clusters encapsulated within LTA zeolites

Trenton Otto [a], Stacey I. Zones [b], Yongchun Hong [a], Enrique Iglesia [a,c,*]

[a] Department of Chemical and Biomolecular Engineering, University of California at Berkeley, Berkeley, CA 94720, USA
[b] Chevron Energy Technology Company, Richmond, CA 94804, USA
[c] Division of Chemical Sciences, E.O. Lawrence Berkeley National Laboratory, Berkeley, CA 94720, USA

ARTICLE INFO

Article history:
Received 19 July 2017
Revised 16 September 2017
Accepted 15 October 2017

Keywords:
Zeolite encapsulation
Cobalt oxide nanoparticles
Cobalt catalyst
Sinter stable
Hydrothermal synthesis
LTA zeolite

ABSTRACT

Small Co_3O_4 nanoparticles uniformly distributed in size were encapsulated within LTA zeolite crystals in a one-step process through hydrothermal self-assembly of crystalline frameworks around ligated Co^{2+} precursors. The use of bifunctional ligands containing a chelating bidentate amine functionality and an alkoxysilane moiety prevented the precipitation of Co^{2+} species as colloidal hydroxides in the highly alkaline synthesis gels, while also allowing the formation of linkages between precursors and the framework during the nucleation and growth of LTA crystals. Oxidative treatments of ligated compounds occluded within zeolite crystals removed ligand residues and formed small Co_3O_4 nanoparticles visible in transmission electron micrographs. These nanoparticles retained their small size (average diameter 1.5 nm) after oxidative treatment at 620–870 K, a reflection of their stabilization by confinement within zeolite voids. The infrared spectra of adsorbed CO on Co-LTA samples confirmed the absence of Co^{2+} as exchanged cations or aluminosilicates, indicating the presence of Co oxide clusters, with dynamics and stoichiometry of reduction in H_2 corresponding to small Co_3O_4 clusters. Ethanol oxidation rates on Co-LTA samples, exchanged with K^+ or Ca^{2+} cations to vary the diffusive properties of LTA crystals, indicated that more than 97% of the active surfaces on these Co_3O_4 clusters resided within zeolite crystals, where ethanol and O_2 concentrations depend on the diffusive properties of the LTA framework. The Co_3O_4 clusters prepared by these methods, in contrast with Co^{2+} in exchanged or aluminosilicate forms, exhibit reactivity in CO and NO oxidation. Their turnover rates (per exposed Co atom), however, were lower than on bulk Co_3O_4 powders, because of the combined effects of diffusional constraints imposed by the confining framework and the small size of these clusters, which leads to lower intrinsic reactivities as a result of their more difficult reduction during catalytic redox cycles. These clusters would be attractive in catalytic applications requiring stability against sintering during reaction or regeneration, reactant or product shape selectivity, or protection from contact with large molecules that block active surfaces. Such oxide clusters cannot be formed by sequential ion exchange, detachment by reduction to Co^0, and re-oxidation because the extremely high temperatures required for reduction destroy the aluminosilicate frameworks. The synthesis protocols and their mechanistic interpretations described herein represent a conceptual and practical platform for the encapsulation of nanoparticles of base elements within a broad range of confining crystalline environments through one-step hydrothermal self-assembly.

Published by Elsevier Inc.

1. Introduction

The synthesis of Co oxide nanoparticles and their applications in heterogeneous catalysis are of interest because they are among the most active catalysts in CO oxidation [1], oxidative dehydrogenation [2], oxidative abatement of volatile organic compounds [3], and alcohol oxidation [4]. Co oxides are also precursors to Co metal particles active in Fischer-Tropsch synthesis catalysis [5]. The structure and size of such clusters influence turnover rates and selectivities for many of these reactions [4,5], and rigorous assessments of their effects on reactivity require the synthesis of clusters that are thermally stable and narrowly distributed in size. Several strategies have been proposed for the synthesis of CoO_x particles; these include incipient wetness impregnation onto mesoporous supports [6,7], sol-gel methods [8], electrochemical deposition of Co^{2+} precursors onto solid substrates [9], and thermal

* Corresponding author at: University of California, Berkeley, 103 Gilman Hall, Berkeley, CA 94720-1462, USA.
E-mail address: iglesia@berkeley.edu (E. Iglesia).

https://doi.org/10.1016/j.jcat.2017.10.017
0021-9517/Published by Elsevier Inc.

decomposition of organometallic precursors in air [10] or under solvothermal conditions [11]. These methods, with some exceptions [7], typically lead to particles >10 nm and broadly distributed in size [6,10]. Cobalt oxide clusters as small as 4 nm have been prepared through incipient wetness impregnation of cobalt precursors into mesoporous MFI zeolite nanosheets [7]. Such clusters reside within the mesoporous regions of the zeolite sheets and take on the size of the mesopores, which confer improved thermal stability to the cobalt oxide clusters relative to particles dispersed on γ-Al_2O_3. Clusters prepared through this technique, however, cannot retain sizes smaller than the mesopores produced natively by the zeolite synthesis (~4 nm) and do not benefit from the molecular sieving or size-selective effects of the zeolite during catalysis, which reflects their location within fully accessible mesoporous regions [7]. The full extent to which the cobalt particles are stabilized by the mesopores against sintering is also unclear. Highly dispersed CoO_x species make efficient use of Co atoms, but tend to sinter at the temperatures and reactive environments required for their use as catalysts [12].

Synthesis techniques that form metal (Au, Pd, Pt) and alloy (AuPd, AuPt, PdPt) nanoparticles within zeolitic voids of molecular dimensions have been shown previously to circumvent the stability and dispersity hurdles inherent to small metal particles [13–15]. Encapsulation within such voids inhibits the mobility and restricts the size of metal clusters [13], while also providing sieving and shape selective effects that allow preferential access to active sites by certain molecules [16], while stabilizing transition states with preferences that sense their fit within the confining voids [13,14]. When so required for catalytic use, such metal clusters can be converted to their corresponding oxides by thermal treatments in O_2. Most aqueous cations of base metals (e.g. Co^{2+}, Mn^{2+}, Ni^{2+}) [17,18], but not the cationic forms of noble metals (e.g. Pd^{2+}, Pt^{2+}, Au^{3+}) [19], can enter small-pore (8 member-ring (MR) apertures), as well as medium-pore (10 MR) and large-pore (12 MR) zeolites. Encapsulation is viable through post-synthesis aqueous ion exchange when solvated precursors can enter the apertures that connect the voids, but exchanged cations of base metals require reductive treatments at temperatures that often lead to significant sintering of the particles formed and to extracrystalline metal agglomerates [17,18]. Co^{2+} cations attached to LTA framework exchange sites, in particular, require treatments in H_2 above 1000 K to form Co^0 metal particles [17].

Here, we describe an alternate strategy to form Co_3O_4 nanoparticles within LTA zeolite crystals; such clusters are small (1.4–1.6 nm) and nearly monodisperse (dispersity index (DI) [20] 1.03–1.07). These protocols prevent the direct attachment of Co^{2+} cations to framework ion exchange sites through the use of ligands that preclude Co^{2+} species from exchange while promoting the self-assembly of the zeolite around Co precursors during hydrothermal crystallization. Bidentate amine ligands (N-[3-(trimethoxysilyl)propyl]ethylenediamine; TPE) chelate Co^{2+} cations to prevent premature $Co(OH)_2$ precipitation in highly alkaline synthesis gels and form siloxane linkages with LTA nuclei to induce their incorporation as crystallization occurs, without interfering with framework crystallinity at Co contents up to 4 wt.%. These Co^{2+}-TPE complexes do not form cation-framework linkages that render Co^{2+} species inert towards the formation of CoO_x clusters during subsequent thermal treatments. Ligands are removed by treatment in O_2 at 623 K, leading to the formation of small and nearly monodisperse Co_3O_4 clusters, resistant to sintering even after O_2 treatment at 870 K.

The temperature and H_2 consumption stoichiometry during reduction confirmed their small size and their Co_3O_4 composition; they reduce at temperatures between those required for the reduction of bulk Co_3O_4 and Co^{2+} exchanged onto LTA. Infrared (IR) spectra did not detect bands for CO bound to exchanged Co^{2+} cations, cobalt silicates, or cobalt aluminates. Ethanol oxidation rates varied as different cations (Na^+, Ca^{2+}, K^+) were exchanged onto LTA crystals to change their intracrystalline diffusivities, consistent with the presence of Co_3O_4 clusters within such crystals. These LTA-encapsulated Co_3O_4 nanoparticles, but not exchanged Co^{2+} cations, were active for CO and NO oxidation, demonstrating their ability to undergo reduction-oxidation cycles and to dissociate molecular oxygen.

These encapsulation strategies, described here for Co-based LTA systems seem generally applicable to other base metals (Cu, Fe, Ni), which form similar stable amine complexes [21] that are essential for stabilization and encapsulation, and to other zeolites (e.g. FAU, EDI, GIS, SOD) that crystallize under hydrothermal conditions similar to those required to form LTA [22].

2. Experimental methods

2.1. Source and purity of reagents used

$CoCl_2{\cdot}6H_2O$ (99.99%, Sigma-Aldrich), $[Co(NH_3)_6]Cl_3$ (99.99%, Sigma-Aldrich), $Co(NO_3)_2{\cdot}6H_2O$ (>98%, Sigma Aldrich), ethylenediamine (98%, Sigma-Aldrich), N-[3-(trimethoxysilyl)propyl]ethylenediamine (TPE; 98%, Sigma-Aldrich), Ludox AS-30 colloidal silica (30 wt.% suspension in H_2O, Sigma-Aldrich), NaOH (99.99%, Sigma-Aldrich), $NaAlO_2$ (53% Al_2O_3, 42.5% Na_2O, Riedel-de Haën), $CaCl_2{\cdot}2H_2O$ (EMD Millipore), KCl (>99.0%, Sigma-Aldrich), Co_3O_4 (99.9%, Sigma-Aldrich), fumed SiO_2 (Davisil Grade 62, Sigma-Aldrich, 300 m^2 g^{-1}), acetone (99.9%, Sigma-Aldrich), ethanol (99.9%, Sigma-Aldrich), air (extra dry; 99.999%, Praxair), H_2 (99.999%, Praxair), He (99.999%, Praxair), Ar (99.999%, Praxair), CO_2 (99.999%, Praxair), N_2 (99.999%, Praxair), 4% H_2/Ar (99.999%, Praxair), 1% CO/He (99.999%, Praxair), CO (99.999%, Praxair), 3% NO/He (99.999%, Praxair), and 1% NO_2/He (99.999%, Praxair) were used as received.

2.2. Materials synthesis

2.2.1. Synthesis of CoO_x clusters within LTA zeolites and cobalt oxide clusters dispersed on SiO_2

LTA was prepared in its Na form (NaLTA) with encapsulated CoO_x species (CoNaLTA) by adding Co cations protected by amine ligands (ammonia, ethylenediamine, or TPE) to zeolite synthesis gels and subsequent hydrothermal crystallization (373 K, 12 h). Syntheses with ethylenediamine or TPE ligands involved the initial dropwise addition of aqueous $CoCl_2{\cdot}6H_2O$ (0.18–0.91 g in 9 cm^3 deionized H_2O, 17.9 Ω cm resistivity) at a rate of 0.2 cm^3 s^{-1} to aqueous ligand solutions (0.09–1.39 cm^3 ethylenediamine or 0.16–1.65 cm^3 TPE dissolved in 9 cm^3 deionized H_2O) while mixing with a magnetic stir bar (6.7 Hz). The amount of ligand used was adjusted for different batches to give ligand/metal molar ratios between 1 and 3. For the case of NH_3 ligands, $[Co(NH_3)_6]Cl_3$ (0.20–1.00 g) was initially dissolved in 18 cm^3 of deionized H_2O. The aqueous solutions of ligands and metal cations were then transferred into 125 cm^3 polypropylene bottles, and colloidal silica (5.3 g, Ludox AS-30) and NaOH (2.4 g) were sequentially added; the containers were sealed and kept at 353 K for 0.5 h with stirring by a magnetic bar (6.7 Hz) and then cooled to ambient temperature. Aqueous $NaAlO_2$ (3.0 g in 9 cm^3 deionized H_2O) was then added, and the mixtures were magnetically stirred (6.7 Hz) for 2 h at ambient temperature. The resulting homogeneous synthesis gels contained molar ratios of 1.7 SiO_2/1 Al_2O_3/3.2 Na_2O/110 H_2O/0.066–0.33 Co/0.066–0.99 ligand. The bottles containing the gels were sealed and the contents heated to 373 K for 12 h while stirring (6.7 Hz) to form as-synthesized CoNaLTA samples.

The Co content in the synthesis gels was chosen to achieve 1–5 wt.% Co in the product solids based on a total yield of ~4.5 g, the approximate yield of NaLTA synthesized without Co using the procedure described here. The solids formed were separated by filtration (Pyrex 3606 fritted funnel, 4–5.5 μm) and washed with deionized water until the rinse liquids reached a pH of 7–8; they were then treated in a convection oven at 373 K for 8 h. The solids were finally heated in flowing dry air (1.67 cm^3 g^{-1} s^{-1}) from ambient to 623 K (at 0.033 K s^{-1}) and held for 3 h. The cobalt content in these samples was measured by inductively-coupled plasma atomic emission spectroscopy (ICP-AES) or estimated from ultraviolet–visible analysis of supernatant liquids after synthesis (Section 2.3.3). Elemental analysis of Si, Al, Na, Ca, and K was also conducted to determine Si/Al ratios (Section 3.1) and cation contents (Section 2.2.2).

Cobalt oxide (Co_3O_4) particles dispersed on mesoporous SiO_2 were prepared and used in CO oxidation and NO oxidation reactions (Section 3.3.2) for comparison with LTA-encapsulated Co oxide clusters. Co/SiO_2 was prepared by incipient wetness impregnation of fumed SiO_2 using aqueous $Co(NO_3)_2$ to achieve 30 wt.% Co loading. The SiO_2 support was heated in flowing air (1.67 cm^3 s^{-1} g^{-1}) at 773 K for 5 h before impregnation; SiO_2 impregnated with $Co(NO_3)_2$ was heated in a convection oven at 400 K for 12 h and then heated again in flowing dry air (1.67 cm^3 g^{-1} s^{-1}) to 773 K (at 0.083 K s^{-1}) and held for 5 h to form Co/SiO_2. This Co/SiO_2 sample was intended for use as a typical supported cobalt oxide catalyst in order to compare its properties with those of the Co-LTA materials considered in this work.

2.2.2. Ion-exchange of CoNaLTA samples with Ca^{2+} and K^+

CoNaLTA (0.4 nm apertures) [23] was fully exchanged with Ca^{2+} cations to form CoCaLTA (0.5 nm) [23] or with K^+ cations to form CoKLTA (0.3 nm) [23] in order to adjust the effective pore diameter of the LTA zeolites before using them in spectroscopic (Section 3.2.5) or catalytic (Section 3.3) experiments. CoNaLTA was also partially exchanged with Ca^{2+} with the intention of replacing half of the exchanged Na^+ ions with Ca^{2+} ions (assuming one Ca^{2+} ion displaces two Na^+ ions) and forming a sample with an effective aperture size between 0.4 and 0.5 nm; such partially exchanged samples are denoted $CoCa_{0.5}Na_{0.5}LTA$. CoCaLTA and CoKLTA were prepared by adding CoNaLTA (1 g) to aqueous $CaCl_2{\cdot}2H_2O$ or KCl solutions (3M; 100 cm^3/g zeolite) and stirring (6.7 Hz) at ambient temperature for 8 h. This exchange process was repeated three times in order to ensure full exchange. $CoCa_{0.5}Na_{0.5}LTA$ samples were prepared by adding CoNaLTA (1.00 g) to an aqueous solution of $CaCl_2{\cdot}2H_2O$ (0.15 M; 9 cm^3/g zeolite) and stirring (6.7 Hz, 24 h) at ambient temperature. The added quantities of CoNaLTA and $CaCl_2{\cdot}2H_2O$ gave a total Na^+/Ca^{2+} ratio of 4 based on the LTA unit cell stoichiometry ($[Na^+_{12}(H_2O)_{27}]_8[Al_{12}Si_{12}O_{46}]_8$) [23]. All samples were filtered and washed with deionized water (1500 cm^3 g^{-1}) after these exchange procedures and then heated in flowing dry air (1.67 cm^3 g^{-1} s^{-1}) from ambient temperature to 623 K (at 0.033 K s^{-1}) and held for 3 h.

Elemental analysis of CoNaLTA (3 wt.% Co) after exchange with K^+ or Ca^{2+} confirmed the essentially full exchange of these cations into the product CoKLTA (K/Al = 0.9) and CoCaLTA (Ca/Al = 0.5) samples. The final Na/Ca ratio measured in the $CoCa_{0.5}Na_{0.5}LTA$ sample (3 wt.% Co; nominal Na/Ca ratio of 2 assuming full Ca^{2+} uptake) was 2.8.

2.2.3. Preparation of Co^{2+}-exchanged LTA

Co-LTA samples were prepared by direct ion-exchange of Co^{2+} cations onto NaLTA to provide comparative samples for the CoNaLTA samples prepared by hydrothermal crystallization (Section 2.2.1). These samples were compared using spectroscopic (Section 3.2.5) and catalytic (Section 3.3) data to determine differences in the type of Co species present in each sample and to confirm the absence of exchanged Co^{2+} cations in CoNaLTA. The exchange was carried out to achieve 3 wt.% theoretical loading by adding 3 g NaLTA (synthesized as in Section 2.2.1 but without ligands or Co precursors) to an aqueous solution of $CoCl_2{\cdot}6H_2O$ (0.36 g in 10 cm^3 H_2O) and stirring (6.7 Hz, 8 h) at ambient temperature. The samples were then filtered, washed, and treated in air as with the CoCaLTA and CoKLTA samples following their ion exchange procedures (Section 2.2.2). The essentially full Co^{2+} uptake into LTA (3 wt.% Co; Co/Al = 0.09) was confirmed by the UV–visible spectra (Section 2.3.3) of the supernatant liquids remaining after contact with LTA.

2.3. Characterization of framework structures and CoO_x particle size and stoichiometry

2.3.1. Powder X-ray diffraction

X-Ray diffractograms (XRD) were used to assess the crystallinity of all samples and to detect any large Co oxide agglomerates (>10 nm) present in CoNaLTA samples. Measurements were carried out using a D8 Discover GADDS Powder Diffractometer with Cu-Kα radiation (λ = 0.15418 nm, 40 kV, 40 mA) over a 2θ range of 5–50° at 0.00625° s^{-1} scan rates. Measurements were conducted on finely ground samples spread as a thin level coating onto quartz slides.

2.3.2. Transmission electron microscopy

Transmission electron microscopy (TEM) was used to measure the distribution of CoO_x cluster sizes. Micrographs were collected using a Philips/FEI Technai 12 microscope at 120 kV by dispersing ground powders in acetone and then onto holey carbon films supported on 400 mesh copper grids (Ted Pella Inc.). Size distributions were measured from >300 particles for each sample and used to determine surface-averaged cluster diameters $\langle d_{TEM} \rangle$ [24]:

$$\langle d_{TEM} \rangle = \frac{\sum n_i d_i^3}{\sum n_i d_i^2} \quad (1)$$

where n_i is the number of clusters with diameter d_i. These size distributions were also used to calculate a dispersity index (DI), defined as the ratio of the surface-averaged ($\langle d_{TEM} \rangle$) to the number-averaged ($\langle d_n \rangle$) mean diameters [24]:

$$DI = \frac{\langle d_{TEM} \rangle}{\langle d_n \rangle} = \frac{\left(\frac{\sum n_i d_i^3}{\sum n_i d_i^2}\right)}{\left(\frac{\sum n_i d_i}{\sum n_i}\right)} \quad (2)$$

DI values provide the accepted metric of size uniformity, with values smaller than 1.5 typically considered to be monodisperse [20].

2.3.3. Ultraviolet–visible spectra of aqueous cobalt cation solutions

The ultraviolet–visible (UV–vis) spectra of the supernatant solutions remaining after hydrothermal CoNaLTA syntheses (Section 2.2.1) were used to estimate the residual concentrations of ligated Co precursors in solution. UV–vis spectra were measured on liquid aliquots held in quartz cuvettes (10 cm^3, Agilent) using a two-beam spectrophotometer (Varian Cary 400 Bio). Spectra were collected in the 450–650 nm wavelength range at scan rates of 5 nm s^{-1}. Aqueous cationic Co species exhibit strong absorption bands in the visible range (400–700 nm) [25]. Calibration curves relating the integrated intensity of these bands to the cobalt species concentrations were prepared using standard solutions of each ligated complex ($Co(NH_3)_6^{3+}$, Co^{2+}/ethylenediamine, Co^{2+}/TPE; Section 2.2.1). Such ligated complexes were dissolved in the

supernatant liquid extracted from cobalt-free NaLTA syntheses in order to obtain reliable absorption cross sections. The volumes and Co concentrations of supernatant solutions from CoNaLTA syntheses were then used to calculate the Co uptake into the product solids formed. The accuracy of this technique was confirmed by comparing the calculated metal loadings to those measured directly with ICP analysis for 1 wt.% and 3 wt.% CoNaLTA samples; the error in the UV–Vis technique, relative to elemental analysis, was <10%.

2.3.4. Temperature programmed oxidation of ligated Co species in Co-LTA zeolites

The formation of combustion products (H_2O, CO_2, N_2, N_2O, NO, NO_2) of ligands was monitored as a function of temperature during treatment of as-synthesized CoNaLTA samples in O_2. These temperature programmed oxidation (TPO) experiments were conducted to identify the stoichiometry of cobalt-ligand attachments and the conditions required for the removal of ligand residues from solid samples. Catalyst samples (0.2 g) were held on a porous quartz frit within a quartz tube (10 mm O.D.) placed in a resistively-heated furnace. Samples were first heated in He (8.3 $cm^3\ g^{-1}\ s^{-1}$) at 373 K for 2 h with the intent to remove physisorbed water and subsequently heated in 10% O_2/He (8.3 $cm^3\ g^{-1}\ s^{-1}$) to 850 K (at 0.167 K s^{-1}). The reactor effluent was analyzed using mass spectroscopy during the latter heating period in O_2; He (4 amu), H_2O (18 amu), N_2 (28 amu), O_2 (32 amu), CO_2 (44 amu), N_2O (44 amu), and NO/NO_2 (30 amu) mass signals were monitored every 10 s (Mini-lab, MKS Instruments, Orion Compact Residual Gas Analyzer; differentially-pumped atmospheric sampling system). Response factors for these species were calculated from calibration experiments using He, O_2, N_2, and CO_2 gases, or by heating in 10% O_2/He flow known quantities of $Co(NO_3)_2$, which thermally decomposes to form precise quantities of NO_x(g) at ~573 K [26].

2.3.5. Temperature programmed reduction of Co species in Co-LTA zeolites

Temperature programmed reduction (TPR) experiments were conducted on CoNaLTA and CoCaLTA samples prepared using hydrothermal methods and ligated Co precursors (Section 2.2.1) and on Co-LTA samples prepared by Co^{2+} exchange (Section 2.2.3) to determine the Co oxidation state and the reduction onset temperature for each sample. TPR experiments were performed using a Micromeritics AutoChem II 2920 analyzer system equipped with a thermal conductivity detector (TCD) to monitor H_2 consumption. Catalyst samples (0.1 g) were loaded in a quartz U-tube reactor and first heated to 313 K in flowing Ar (0.83 $cm^3\ s^{-1}$) for 0.33 h. The Ar was then replaced with 4% H_2/Ar (0.83 $cm^3\ s^{-1}$) and the samples were heated (at 0.167 K s^{-1}) to 1273 K while the TCD signal in the reactor effluent was continuously monitored. The H_2 response factor for the TCD was determined by treating known amounts of Co_3O_4 to form Co metal while measuring the amount of H_2 consumed.

2.3.6. Infrared spectra of adsorbed CO on cobalt-LTA zeolites

The infrared (IR) spectra of CO adsorbed on CoCaLTA and Co^{2+}-exchanged LTA samples were collected in order to detect exchanged Co^{2+}, cobalt silicate, or cobalt aluminate species. The exchange of monovalent Na^+ cations in NaLTA with divalent cations (e.g., Ca^{2+} or Co^{2+}) decreases the total number of cation species in the framework and effectively widens LTA apertures, thus allowing more facile access by CO(g) to intracrystalline voids [13]. The Ca^{2+} exchanged form (CoCaLTA) of the hydrothermally prepared samples was therefore used for these IR experiments. IR spectra were acquired in transmission mode on wafer samples (40 mg cm^{-2}) using a Thermo Nicolet 8700 spectrometer equipped with an in-situ flow cell. Wafers were first heated in flowing He (40 $cm^3\ g^{-1}\ s^{-1}$) from ambient temperature to 473 K (at 0.033 K s^{-1}) and held for 1 h. The samples were then allowed to cool in flowing He to 313 K, and the He was replaced with 1% Co/He (40 $cm^3\ g^{-1}\ s^{-1}$). The wafers were exposed to flowing CO for 0.25 h before spectra were collected. The temperature and CO pressures were chosen in order to minimize coverages by physisorbed species and the adsorption of CO onto Ca^{2+} centers in CoCaLTA [13], which could interfere with the accurate assessment of the bands for CO adsorbed onto exchanged Co^{2+} cations. Contributions to the IR absorption from CO(g), though minimal, were subtracted from the reported spectra.

2.3.7. Catalytic assessment of reactivity and encapsulation

Ethanol (EtOH) oxidation turnover rates were measured on CoNaLTA, $CoCa_{0.5}Na_{0.5}$LTA, CoCaLTA, and CoKLTA catalysts that were first diluted (10-fold by mass) with mesoporous SiO_2 and pelleted and sieved to retain 180–250 μm aggregates. Catalyst samples were held on a porous quartz frit within a quartz tube (10 mm O.D.) and treated in 20% O_2/He (1.67 $cm^3\ g^{-1}\ s^{-1}$) at 573 K for 1 h before cooling to reaction temperatures (423–523 K) for rate measurements. Temperatures were controlled using a three-zone resistively-heated furnace; each zone was controlled with a Watlow Series 988 electronic controller. A K-type thermocouple (Omega) attached to the exterior of the quartz tubular reactor was used to measure temperatures. Liquid EtOH was evaporated into flowing O_2/He streams at 393 K using a liquid syringe pump (Cole Parmer, 60061 Series); mass flow controllers (Porter Instrument) were used to adjust O_2 and He flowrates in order to achieve the desired reactant pressures (4 kPa alkanol, 9 kPa O_2, and 88 kPa He). EtOH conversions were kept below 3% to maintain differential conditions suitable for rate measurements, and transfer lines were maintained at ~400 K to avoid condensation of EtOH or its reaction products.

Turnover rates are reported as the molar EtOH conversion rates per surface Co atom. The number of surface Co atoms present in each sample was estimated using the metal loading and cluster dispersion calculated from the surface-averaged nanoparticle diameter (Eq. (2)), the bulk atomic density of Co atoms in Co_3O_4 (45 nm^{-3}) [27], and the surface density of fully exposed Co atoms on the (1 0 0) surface plane in bulk Co_3O_4 (6.1 nm^{-2}) [27]. Cobalt oxide clusters were assumed to be quasi-spherical. Effluent concentrations were measured using a Shimadzu GC-2014 gas chromatograph equipped with a methyl-silicone capillary column (HP-5; 50 m × 0.32 mm, 1.05 μm film thickness) and a flame ionization detector. Catalyst deactivation was not detected in the time scale of the rate measurements (~1–5 h). Experiments using empty reactors, mesoporous SiO_2, and Co-free LTA with Na^+ (NaLTA), Ca^{2+} (CaLTA), or K^+ (KLTA) counterions did not lead to detectable EtOH conversion levels.

The aperture size available for diffusion of molecules into LTA zeolites varies with the number and ionic radius of the charge-balancing cations exchanged into the framework (e.g. KLTA: 0.3 nm, NaLTA: 0.4 nm, CaLTA: 0.5 nm) [23]. Larger cations (e.g. K^+, 0.137 nm) [28] occupy a larger fraction of the intracrystalline space than smaller cations (Na^+, 0.99 nm) [28], thus leading to smaller apertures throughout the LTA framework. Multi-valent cations (Ca^{2+}, 0.100 nm) [28] lead to cation to Al ratios lower than unity and to larger apertures than for monovalent cations. These variations in aperture size lead to more facile diffusion, specifically in this case for EtOH (0.40 nm kinetic diameter [24]) when Ca^{2+} replaces Na^+ or K^+ cations in Co-LTA samples. Rates of EtOH consumption are expected to increase monotonically with effective aperture size if (i) active CoO_x surfaces reside within the zeolite crystallites and (ii) reaction rates are limited by diffusion. A trend of increasing EtOH oxidation rates across samples with

monotonically larger apertures would indicate that CoO_x clusters reside predominantly within LTA crystals.

2.3.8. Assessment of Co-LTA samples as catalysts for CO and NO oxidation

The reactivity of CoNaLTA, CoCaLTA, Co/SiO_2, and Co^{2+}-exchanged LTA catalysts was examined in CO and NO oxidation reactions. Oxidation rates were measured on catalyst samples (100 mg, 180–250 μm aggregates) diluted with quartz granules (100–900 mg; 180–250 μm aggregates) packed in a stainless steel tubular reactor (6.35 mm ID) for CO oxidation or held on a quartz frit in a quartz tube (10 mm OD) for NO oxidation. Samples were treated in flowing 20% O_2/He (0.83 cm^3 s^{-1}) at 573 K for 1 h, and then brought to the reaction temperature (473–633 K) for rate measurements. Temperatures were measured using a type K thermocouple and adjusted by resistive heating using a temperature controller (Watlow, 96 Series). Gas reactants (CO, NO, NO_2 He, O_2) were metered by electronic flow controllers (Porter Instrument) to achieve the desired reactant pressures and total flowrate for CO oxidation (1 kPa CO, 10 kPa O_2, 90 kPa He, 0.83 cm^3 s^{-1}) or NO oxidation (0.1 kPa NO, 0.3 kPa NO_2, 5 kPa O_2, 96 kPa He, 0.83 cm^3 s^{-1}). Reactant (CO and O_2) and product (CO_2) concentrations for CO oxidation reactions were measured by gas chromatography (Agilent 6890 GC) using a Porapak Q packed column (80–100 mesh, 1.82 m × 3.18 mm) with a thermal conductivity detector. CO conversions were below 20% in all experiments. For NO oxidation, samples were exposed to reactants at the reaction temperature for 0.5 h before rate measurements. The reactor inlet and outlet NO and NO_2 concentrations were measured using an infrared analyzer (MKS Multi Gas Analyzer 2030, 2 cm^3 cell; 2 cm path length, 353 K). Measured NO conversions were below 20% for all samples. Plug-flow reactor formalisms were used to correct for changes in reactant concentrations along the catalyst beds and report turnover rates at inlet conditions. CO and NO turnover rates are reported as molar CO or NO conversion rates normalized by the number of surface Co atoms.

3. Results and discussion

3.1. Effects of synthesis protocols on LTA crystallinity and phase purity and Co retention

CoNaLTA samples were prepared using different ligand species and a range of ligand/Co^{2+} ratios (1, 2, 3, and 6) and Co concentrations (1–5 wt.% nominal Co loading) in order to probe the effects of these variables on metal uptakes and LTA crystallinity and, in doing so, to infer the nature of the processes that enforce encapsulation. Ligand species were chosen based on their ability (i) to prevent the precipitation of Co^{2+} cations as colloidal hydroxides at the pH and temperature of LTA synthesis, (ii) to promote the uptake of ligated precursors within LTA crystals, and (iii) to minimize any interference with the crystallization and phase purity of the LTA framework. The results of these studies are summarized in Table 1.

Synthesis gels (pH > 14) were prepared using $[Co(NH_3)_6]Cl_3$ precursors (i.e.·NH_3 ligands) to achieve 1 wt.% nominal Co loading; the resulting suspensions changed from orange to black immediately upon heating to 373 K, consistent with the facile detachment of NH_3 ligands and the consequent precipitation of Co oxyhydroxides in such highly alkaline media. CoNaLTA syntheses using ethylenediamine ligands at ligand/Co^{2+} ratios of 3 showed no color changes that would indicate metal precipitation; these precursors led to the formation of crystalline LTA (XRD; Supporting Information (SI), Section S1) without detectable CoO_x diffraction lines in the solid products formed.

The stability of these ligated Co^{2+} complexes during hydrothermal LTA crystallization reflects the chelation effects conferred by the bidentate ethylenediamine moieties. Their incorporation into the solid products (from UV–vis spectra of supernatant liquids; Section S2), however, was not complete (~40% uptake of the Co^{2+} into the product), indicating that LTA crystals can nucleate and grow around ethylenediamine-Co^{2+} complexes, but without the selectivity required for their full retention within the solids formed. Such limitations were addressed by using N-[3-(trimethoxysilyl)propyl]ethylenediamine (TPE) ligands that include a bidentate amine function, but also an alkoxysilane moiety, intended as a strategy for the formation of siloxane bridges that attach the ligated precursors to silicate oligomers during LTA nucleation and growth. CoNaLTA samples synthesized using TPE at ligand/Co^{2+} ratios of 3 and 1 wt.% nominal Co contents were crystalline (XRD; Section S1) and free of prematurely precipitated CoO_x agglomerates; these ligands also led to the uptake of >90% of the Co atoms in the synthesis reagents into the crystalline LTA solids. This marked improvement in metal uptakes indicates that the alkoxysilane moiety in TPE served its intended purpose as a linkage to incipient LTA frameworks without compromising Co^{2+} stability at high pH or the product LTA crystallinity.

The influence of TPE/Co^{2+} ratios (1, 2 and 3) on the stability of ligated Co^{2+} species, Co retention in product solids, and LTA crystallinity was examined for samples with nominal Co loadings of 1 wt.% TPE/Co^{2+} ratios of 2 and 3 did not affect the stability of

Table 1
Ligand species, ligand/Co ratios, nominal metal loading, metal uptake into solids, stability of ligated cobalt cations in LTA synthesis gels, and crystallinity of synthesized solids for the synthesis of CoNaLTA samples.

Ligand[a]	Nominal metal loading (wt.%)[b]	Ligand/Co ratio[c]	Precursor Stability[d]	% Metal uptake[e]	Crystalline LTA Product?[f]
NH_3	1	6	Unstable	–	–
Ethylenediamine	1	3	Stable	40	Yes
TPE	1	1	Unstable	–	–
TPE	1	3	Stable	90	Yes
TPE	1	2	Stable	90	Yes
TPE	2	2	Stable	90	Yes
TPE	3	2	Stable	90	Yes
TPE	4	2	Stable	90	Yes
TPE	5	2	Stable	90	No

[a] Ligand species used to stabilize Co cations in LTA synthesis gels.
[b] Metal loading that would be achieved if all of the Co added to the synthesis gel were incorporated into the synthesized solids, assuming a solids yield equivalent to a metal and ligand-free NaLTA synthesis.
[c] Molar ratio of ligand/metal added to the synthesis gel.
[d] Unstable ligated cobalt precursors precipitate to form black solids in the LTA synthesis gel prior to the completion of crystallization; stable precursors retain their bright coloration and do not precipitate.
[e] Actual metal uptake in the isolated solids formed after crystallization, calculated using UV–Vis measurements of Co complex concentrations in supernatant solutions.
[f] Determined using XRD.

Co^{2+} against precipitation (no detectable precipitation in LTA synthesis gels (Section 2.2.1) at 373 K), LTA crystallinity (XRD; Section S1), or Co retention in solids (~90%). Lower ratios (TPE/Co^{2+} = 1), however, led to the precipitation of the Co precursors in the synthesis gels at the crystallization temperature (373 K). These data suggest that more than one TPE ligand must coordinate with a Co^{2+} cation to provide the requisite stability, while two TPE ligands are sufficient. Additional ligands may be unable to coordinate at the Co^{2+} center because of steric or electronic consequences brought forth by additional ligand coordination. These data indicate that TPE/Co^{2+} ratios of 2 are sufficient for stability, crystallinity, and Co retention within LTA crystals.

CoNaLTA samples were prepared with a TPE/Co^{2+} ratio of 2 and 1–5 wt.% Co (nominal) in the synthesis gels in order to determine how metal loading influences LTA crystallinity and Co retention selectivity. Retention selectivities remained at ~90% for 1–5% Co contents based on UV–vis absorption measurements of supernatant solutions (Section 2.3.3). Solids with 1% and 3% Co loading also exhibited sharp diffraction lines for LTA crystals (Fig. 1). These lines became broader for the sample with 4% Co, while the 5% sample gave a broad background characteristic of amorphous solids, suggesting that ligated precursors, when present at these higher precursor loadings, can disrupt LTA nucleation and growth. The number of Co atoms per LTA α-cage in 1 and 3 wt.% CoNaLTA samples (assuming one α-cage in the $([Na^{+}_{12}(H_2O)_{27}]_8[Al_{12}Si_{12}O_{46}]_8)$ lattice [23]) are approximately 3 and 9, respectively. The size of the LTA α-cage (1.1 nm void diameter) [24], however, is of similar diameter as a Co^{2+} cation with two attached TPE ligands (~1 nm, estimated using MolView, v. 2.2, largest dimension) [29], the number of ligands determined in Section 3.2.1 from the products evolved during oxidative treatments. Thus, 3–9 Co atoms, each with two attached TPE ligands, cannot reside within each LTA α-cage. Yet, EtOH oxidation reactivity studies (Section 3.3.1) indicate that most Co oxide species reside within the intracrystalline LTA voids, as also shown by the small and uniform Co_3O_4 clusters evident in transmission electron micrographs (Section 3.2.2) after oxidative treatments, which cannot be predominantly located at the low external surface areas of LTA crystals. Micropore volume and surface area measurements (Section S3) conducted on such oxidatively treated CoNaLTA (0.32 $cm^3\ g^{-1}$; 1030 $m^2\ g^{-1}$) and CoCaLTA (0.27 $cm^3\ g^{-1}$; 880 $m^2\ g^{-1}$) samples (3 wt.% Co; CoCaLTA formed from Ca^{2+} ion exchange, Section 2.2.2) were similar to metal-free NaLTA (0.34 $cm^3\ g^{-1}$; 1090 $m^2\ g^{-1}$) and CaLTA (0.29 $cm^3\ g^{-1}$; 970 $m^2\ g^{-1}$) samples, further confirming that the zeolite micropore structure remains intact despite the presence of these cobalt oxide particles within the crystallites. Si/Al ratios for crystalline NaLTA and 3 wt.% CoNaLTA samples, measured using elemental analysis (Section 2.2.1), were 0.98 and 1.02, respectively.

We surmise that the ligated Co^{2+} moieties reside within cavities larger than the α-cages, but still present within LTA crystals, leading to localized disruptions of the crystal lattice without compromising the integrity of the crystallites. When present as small fractions of the crystal volume, nucleation and growth can proceed unaffected, and the subsequent removal of the ligands during oxidative treatments leads to Co_3O_4 clusters and to the healing of the framework in the surrounding larger voids; such clusters remain protected from the external fluid phase by the diffusional barriers imposed by the many intervening windows between such clusters and the LTA external surfaces. These results provide the required guiding principles for preparing ligated Co species occluded within LTA crystals; these species act as convenient precursors to encapsulated Co_3O_4 clusters, suitable as size-selective catalysts (Sections 3.2 and 3.3). The selective retention of ligated Co species requires ligands that simultaneously stabilize metal cations in alkaline media and act as nucleation centers for crystallization; the Co loading, however, is inherently limited by the ability of the frameworks to assemble in the presence of high concentrations of ligated complexes that locally disrupt the LTA crystal periodicity. In the next section, we discuss the process by which such ligated Co species can be converted into encapsulated Co_3O_4 clusters.

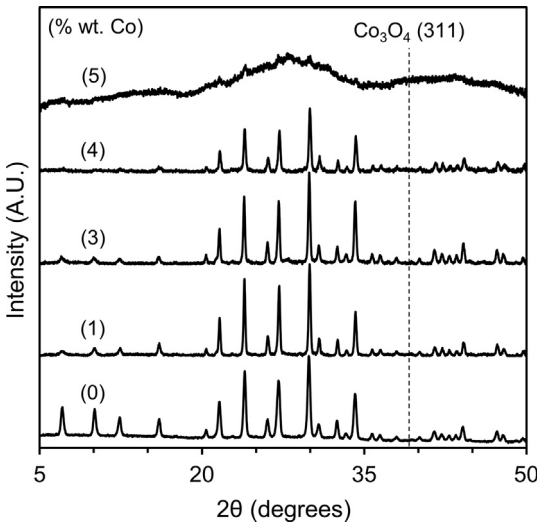

Fig. 1. X-Ray diffractograms for as-synthesized NaLTA and CoNaLTA samples prepared to achieve 0–5 wt.% Co loading in the product solids assuming full metal uptake. Samples prepared with TPE/Co^{2+} ratio of 2.

3.2. Characterization of Cobalt-LTA samples

3.2.1. Temperature programmed oxidation studies of as-synthesized Cobalt-LTA samples

As-synthesized CoNaLTA samples (discussed in Section 3.1; 1 and 3 wt.% Co) were treated in O_2 with the intent of removing TPE ligands and forming CoO_x clusters. Such clusters would be expected to form if the ligated complexes precluded the formation of direct Co^{2+}-framework linkages that would render Co^{2+} species inert towards the formation of oxide clusters. The evolution of the products of ligand decomposition and oxidation was monitored by mass spectroscopy as 1 and 3 wt.% CoNaLTA samples were heated in 10% O_2/He to 850 K (at 0.167 K s^{-1}; Section 2.3.4) in order to determine the Co-ligand stoichiometry and the conditions required for complete removal of the ligands. The TPO profile for 3 wt.% CoNaLTA is shown in Fig. 2 (1 wt.% Co sample in SI, Section S4). H_2O, CO_2, N_2, and NO were detected during these treatments; their rates of formation reached a sharp maximum at ~623 K, and ligand decomposition was essentially complete by 750 K (Fig. 2). N/Co and C/Co ratios calculated for 3 wt.%. CoNaLTA were 3.8 ± 0.4 and 10.5 ± 0.7 (3.9 ± 0.4 and 9.6 ± 0.7 for 1 wt.% sample) respectively, consistent with the presence of two TPE ligands per Co atom and with their full removal during thermal treatment. These data were used to select post-synthesis treatments required to decompose ligated precursors (Section 2.2.1; treatment in dry air at 623 K, 3 h); decomposition products were not detected upon further treatment of these samples in 10% O_2/He to 850 K, consistent with the prior full removal of all C, N, and H atoms introduced as part of the TPE ligands.

Diffuse reflectance ultraviolet–visible (DR UV–vis) spectra (Section S5) were acquired on as-synthesized CoNaLTA, Co^{2+}-exchanged LTA (Section 2.2.3), and oxidatively treated CoNaLTA samples to further demonstrate that oxidative treatment removes the ligands attached to Co^{2+} cations in CoNaLTA, and that such

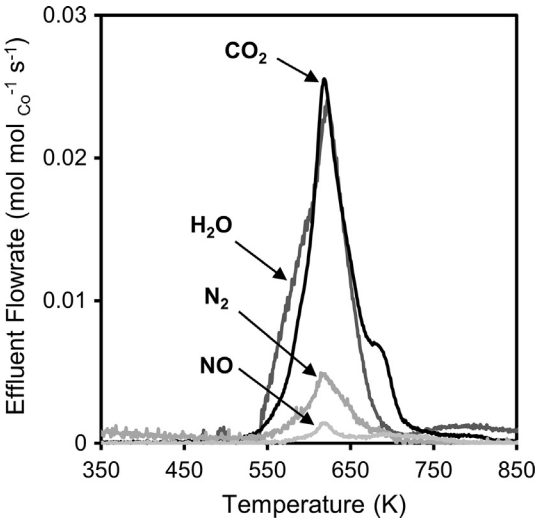

Fig. 2. Effluent gas flowrates calculated from mass signals for H_2O (18 amu), CO_2 (44 amu), N_2 (28 amu), and NO (30 amu) monitored during the thermal treatment of as-synthesized 3 wt.% CoNaLTA with 10% O_2/He (0.83 $cm^3\ g^{-1}\ s^{-1}$) from 350 K to 850 K (at 0.167 K s^{-1}).

treatment leads to the formation of cobalt oxides. The absorption spectrum of as-synthesized CoNaLTA showed ligand to metal charge transfer and d-d transition bands originating from the ligated Co^{2+} cations in the sample (Section S5). Such bands were absent in oxidatively treated CoNaLTA, consistent with the removal of TPE ligands attached to Co^{2+} cations and the formation of CoO_x species during oxidative treatment (Section S5). Co^{2+}-exchanged LTA showed an intense d-d transition feature characteristic of Co^{2+} cations attached to zeolite exchange sites; similar features were not apparent in the spectra of as-synthesized and oxidatively treated CoNaLTA, consistent with the absence of exchanged Co^{2+} cations in those samples. These DR UV–vis spectra are therefore consistent with TPO results indicating the removal of TPE ligands from CoNaLTA during oxidative treatment, and further indicate the prevalence of different coordination environments for Co species in as-synthesized CoNaLTA, oxidatively treated CoNaLTA, and Co^{2+}-exchanged LTA samples.

3.2.2. Assessment of CoO_x cluster sizes after oxidative treatment of as-synthesized Co-LTA samples

Transmission electron microscopy (TEM) was used to detect the presence of any Co-derived nanoparticles after oxidative treatments and to determine the size of such particles in CoNaLTA and in these samples after Ca^{2+} or K^+ exchange (to form CoCaLTA, $CoCa_{0.5}Na_{0.5}$LTA, or CoKLTA; Section 2.2.2). Fig. 3 shows electron micrographs, cluster size distributions, and dispersity indices (DI; Eq. (2)) in these samples. Small clusters were evident in all samples, with surface-averaged diameters (Eq. (1)) of ~1.5 nm and narrow size distributions (DI 1.03–1.07). The dispersions of these clusters range from 0.51 (for $\langle d_{TEM}\rangle$ = 1.6; Eq. (1)) to 0.58 (for $\langle d_{TEM}\rangle$ = 1.4; Eq. (1)) (Section 2.3.7). Their reduction profiles (Section 3.2.4) and infrared spectra (IR; Section 3.2.5) indicate that such particles consist of small Co_3O_4 crystallites; they are somewhat larger than the α-cages in LTA (1.1 nm) [24], indicating that they reside within local disruptions of the LTA framework, which do not affect, however, the long-range periodicity of the zeolite crystals (X-ray diffractogram of air-treated CoNaLTA in Section S1). The small and uniform size of these clusters indicates that ligated precursors were uniformly distributed within the gel precursors as LTA crystals formed, leading to a high density of nucleation points during ligand removal. Mean cluster sizes were similar in 1 wt.% (1.4 nm) and 3 wt.% (1.6 nm) CoNaLTA samples (actual Co contents 0.90 wt.% and 2.64 wt.% by ICP), as also found for the case of Au clusters within LTA [13]. Such size "limits" may reflect the compensating energies inherent in metal oxide cluster growth to decrease surface energy [30] and in the disruption of the LTA framework required to accommodate clusters larger than the native α-cages in LTA frameworks.

Co-LTA prepared by the direct exchange of Co^{2+} cations (Section 2.2.3), in contrast with CoNaLTA prepared by hydrothermal methods (Section 2.2.1), did not show any CoO_x agglomerates in micrographs, even after thermal treatments in flowing dry air at 623 K. These data suggest that the TPE ligands coordinated to the Co^{2+} precursors preclude the formation of linkages between Co cations and the zeolite framework; in doing so, these ligands allow the formation of CoO_x clusters after oxidative treatments. Such clusters are suitable as catalysts for redox reactions involving lattice O-atoms, while exchanged Co cations are essentially unreactive as catalysts for such transformations. These conclusions are consistent with the infrared spectra of bound CO shown below in Section 3.2.5.

3.2.3. Thermal stability of cobalt oxide clusters in LTA

Nanoparticles confined within microporous networks (e.g., Au, Pd, Pt) [13–15,24] show exceptional resistance to coalescence and form larger particles at much higher temperatures than those of similar size dispersed on mesoporous silicates. Such properties reflect kinetic hurdles to migration and thermodynamic effects that balance the lower surface energy of larger crystallites with the required disruptions of the encasing framework.

The thermal stability of CoO_x nanoparticles in CoNaLTA samples was assessed from TEM-derived size distributions (Fig. 3) for CoNaLTA samples (1 and 3 wt.% Co) treated in flowing dry air (1.87 $cm^3\ s^{-1}\ g^{-1}$) by heating to temperatures between 623 K and 1023 K (at 0.033 K s^{-1}) and holding for 3 h. Surface-averaged cluster diameters ($\langle d_{TEM}\rangle$; Eq. (1)) and dispersity indices (DI; Eq. (2)) for 3 wt.% CoNaLTA after these treatments are shown in Fig. 4 (1 wt.% sample in SI, Section S6). Thermal treatments up to 873 K did not lead to any detectable changes in $\langle d_{TEM}\rangle$ (1.5 nm for 1%; 1.6 nm for 3%) or DI (1.07 for 1%; 1.06 for 3%) values for both loadings, consistent with the retention of cluster sizes and their monodispersity. Treatment at temperatures of 973 K or greater, however, led an increase in cluster size (to 3.7 and 4.4 nm for 1% and 3% at 1023 K) and dispersity indices (1.34 and 1.40 for 1% and 3% at 1023 K). This increase in cluster size coincides with the thermal decomposition of the LTA structures at 1023 K (XRD; Section S7), suggesting that intact frameworks are essential to stabilizing the highly dispersed cobalt oxide clusters. We will show in Section 3.2.5 through IR studies that thermal treatment at 1020 K also causes a significant fraction of the CoO_x nanoparticles to react with the decomposed residues of the framework and form Co aluminosilicates.

The weak effects of metal content on cluster size and stability suggest that the LTA framework, when intact, imposes a limit on the size to which CoO_x clusters can grow. Such limits would favor a high density of nucleation points in high-loading samples and, consequently, small CoO_x clusters of size insensitive to Co content. We surmise that constraints to cluster growth include kinetic limits to metal oxide mobility imposed by the intervening apertures and thermodynamic barriers arising from the energy needed to distort the framework in regions surrounding the particles to allow cluster growth. These considerations and unique stability would require the predominant presence of such clusters within LTA crystallites, which preserve such clusters at conditions that would otherwise lead to their extensive growth. More direct evidence of encapsulation is presented in Section 3.3.1 from diffusional effects on the reactivity of these samples for ethanol oxidation.

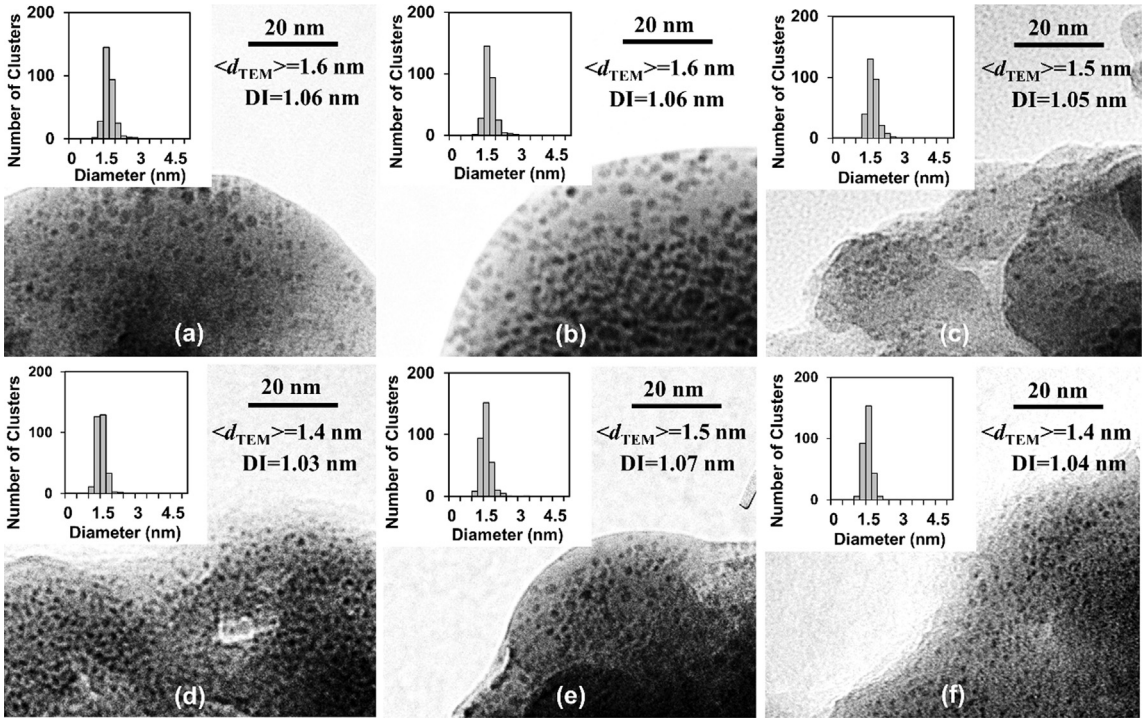

Fig. 3. Transmission electron micrographs, surface-averaged cluster diameters (⟨d_{TEM}⟩, Eq. (1)), particle dispersity indices (DI, Eq. (2)), and cluster diameter distributions for (a) CoCaLTA, (b) CoNaLTA, and (c) CoKLTA samples with 3 wt.% Co loading and (d) CoCaLTA, (e) CoNaLTA, and (f) CoKLTA samples with 1 wt.% Co loading.

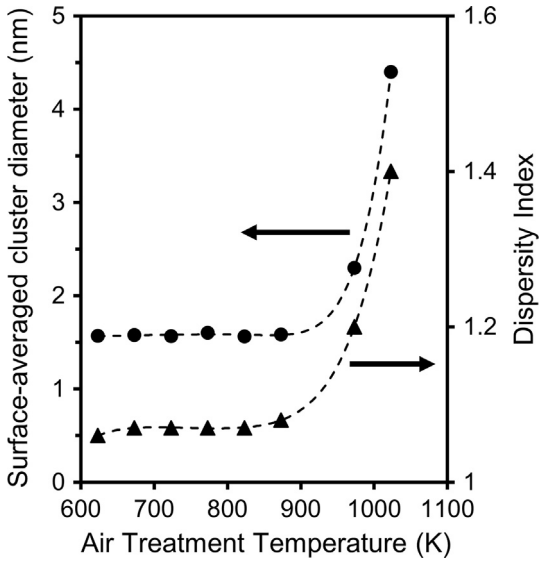

Fig. 4. Effect of flowing dry air treatment temperature (1.67 $cm^3\ g^{-1}\ s^{-1}$, 3 h) on the TEM[-derived surface-averaged cluster diameter (●; Eq. (1)) and Dispersity Index (▲; Eq. (2)) of cobalt oxide clusters in CoNaLTA (3 wt.% Co loading).

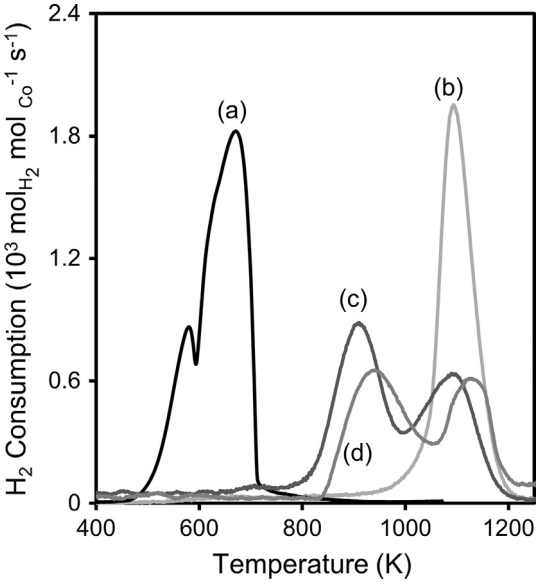

Fig. 5. Temperature programmed reduction (TPR) profiles of (a) Co_3O_4, (b) 3 wt.% Co^{2+}-exchanged LTA, (c) 3 wt.% CoNaLTA, and (d) 3 wt.% CoCaLTA samples heated in 4% H_2/Ar (8.3 $cm^3\ s^{-1}\ g^{-1}$) from 313 K to 1273 K at 0.167 K s^{-1}.

3.2.4. Reducibility of cobalt species in cobalt-LTA samples

The oxidation state and reduction dynamics of Co species in CoNaLTA and Co^{2+}-exchanged LTA were determined using temperature-programmed reduction (TPR) methods involving treatment in 4% H_2/Ar from 313 K to 1273 K (at 0.167 K s^{-1}) and measurements of H_2 consumption by thermal conductivity (Section 2.3.5). The full reduction of zeolite-exchanged Co^{2+} species requires temperatures above 1000 K [17], while bulk Co_3O_4 and CoO reduce at much lower temperatures (473–673 K) [31]. Small CoO_x domains are more resistant to reduction in H_2 than larger crystallites, a trend typically attributed to stabilization of oxides by interactions with the support [5,32,33] or to larger HOMO-LUMO gaps in highly dispersed semiconducting oxides [34]. CoO_x and exchanged Co^{2+} species on silicates (e.g. mesoporous SiO_2, MCM-41) [31,35,36] and aluminates (e.g. Al_2O_3) [37] also form Co—O—Si or Co—O—Al linkages upon thermal treatments in air or H_2 to temperatures above 900 K, because of the formation of Co_2SiO_4 or $Co_2Al_2O_5$ crystallites that require very high temperatures (and significant growth) for their full reduction in H_2 (>900 K)

[35,37]. These temperatures approach the stability limits of the LTA structure and most other zeolite frameworks (~1000 K) [38].

Fig. 5 shows reduction profiles for bulk Co_3O_4, 3 wt.% CoNaLTA, 3 wt.% CoCaLTA, and Co^{2+}-exchanged LTA (3 wt.% Co; Section 2.2.3). The onset of bulk Co_3O_4 reduction appeared at ~500 K and showed two features with H_2/Co consumption ratios of 0.33 ± 0.03 and 1.00 ± 0.08, corresponding to the sequential reduction of Co_3O_4 to CoO and then to Co^0 [31]. Co^{2+}-exchanged LTA samples gave a single feature starting at a much higher temperature (~1000 K), consistent with the presence of refractory Co^{2+} cations linked to Si or Al atoms in the framework [17] or Co aluminosilicates [35,37]. The H_2/Co consumption ratio (1.06 ± 0.08) was that expected from the reduction of all Co^{2+} cations exchanged onto LTA. CoNaLTA and CoCaLTA prepared via hydrothermal assembly (Section 2.2.1) each gave two reduction features; the first feature (onset at ~ 800 K) appears at a much higher temperature than in bulk Co_3O_4 (500 K), consistent with the high dispersion of the CoO_x clusters. The second feature (onset at ~1000 K) resembles that for Co^{2+}-exchanged LTA. Such similarities may indicate that some Co species exchanged during hydrothermal synthesis of CoNaLTA or that exposure to these high temperatures lead to LTA structural degradation, loss of confinement, and the consequent formation of Co silicates or aluminates. The absence of the CO IR bands expected for exchanged Co^{2+}, cobalt aluminates, and cobalt silicates in CoCaLTA (Section 3.2.5) rules out their formation during synthesis or post-synthesis air treatment at 623 K (Section 2.2.1). We will show that the much higher temperatures used during TPR (~1000 K) lead to the degradation of the zeolite and to structural rearrangements that favor the formation of dense mixed oxide structures (Section 3.2.5); the reduction of Co cations within such structures account for the H_2 consumption feature centered at ~1100 K.

The total H_2/Co consumption ratios for CoNaLTA and CoCaLTA were slightly larger than unity (1.16 ± 0.09 and 1.14 ± 0.09, respectively), as expected from the presence of Co^{3+} species as Co_3O_4. The presence of Co_3O_4 was also confirmed by CO oxidation rates (Section 3.3.2), that depend on the tendency of Co^{3+} to undergo reduction-oxidation cycles [39]. The H_2/Co ratios are lower than expected from pure Co_3O_4 (1.33), indicating that some Co^{2+} species are present as CoO. The Co_3O_4 phase is thermodynamically favored in bulk CoO_x compounds at ambient O_2 pressures below ~1100 K [40]; however, small CoO clusters can persist in oxidizing environments well below this temperature [11], which may reflect hurdles imposed by nucleation barriers or thermodynamics that favor CoO in small clusters because of surface energy considerations. About half of the H_2 is consumed as part of the low-temperature feature (800 K; H_2/Co ratios of 0.66 ± 0.08 and 0.64 ± 0.08 for CoNaLTA and CoCaLTA), suggesting that CoO_x clusters can be partially reduced before their conversion to cobalt aluminosilicates and their ultimate reduction at higher temperatures. These reduction profiles are consistent with the presence of highly dispersed CoO_x clusters in CoNaLTA and CoCaLTA samples after their post-synthesis air treatment at 623 K (Section 2.2.1), though the additional presence of some exchanged Co^{2+} cations or Co aluminosilicates cannot be excluded using these data alone. In the next section, evidence is presented to confirm the absence of such Co species using infrared spectroscopy.

3.2.5. Identification and assessment of Co species within cobalt-LTA zeolites by infrared spectra of chemisorbed CO

The infrared spectra of CO adsorbed on CoCaLTA, Co_3O_4, and Co^{2+}-exchanged LTA was used to detect the presence of exchanged Co^{2+} and Co aluminosilicates. The CoNaLTA samples (0.4 nm apertures) [23] were first exchanged with Ca^{2+} to form CoCaLTA (0.5 nm apertures) [23], so as to allow CO diffusion at the mild temperatures (~300 K) required for detectable CO coverages (Section 2.2.2) [13]. UV–vis spectra (Section 2.3.3) of the supernatant liquids during Ca^{2+} exchange of CoNaLTA did not detect any leached Co^{2+} species. The infrared spectra of CO adsorbed on CoCaLTA (3 wt.% Co; $\langle d_{TEM} \rangle$ = 1.6 nm), Co^{2+}-exchanged LTA (3 wt.% Co), and Co_3O_4 at 313 K and 1 kPa CO are shown in Fig. 6.

The Co^{2+}-exchanged LTA sample shows an intense infrared band at 2180 cm^{-1}, attributed to CO at exchanged Co^{2+} species in zeolites [41,42], while the bulk Co_3O_4 sample did not show comparably intense features in the carbonyl frequency range (1900–2400 cm^{-1}) [41–44]. CoCaLTA also did not show significant bound CO features upon contact with CO(g), indicative of the absence of accessible exchanged Co^{2+} cations, Co silicates, or Co aluminates, which bind CO and would have given intense CO stretches between 2150 and 2200 cm^{-1} [45–47]. CoCaLTA samples heated in air or H_2 to 1020 K, however, showed absorption bands at 2175 cm^{-1} (Section S7) and significant structural degradation (XRD; Section S7), consistent with LTA decomposition and consequent formation of Co aluminosilicates at these temperatures. The formation of these refractory Co aluminosilicates account for the high temperature reduction feature in TPR (at ~1100 K; Section 3.2.4). The absence of significant infrared bands for CO physisorbed on Co_3O_4 [44] or adsorbed on Ca^{2+} cations in CoCaLTA [13,41] reflects the very low CO pressures (1.0 kPa) and modestly high temperatures (313 K) used. These data, taken together with TEM (Section 3.2.2) and TPR (Section 3.2.4) evidence, show that ligated precursors prevent the formation of exchanged Co^{2+} species or Co aluminosilicates during hydrothermal synthesis of CoNaLTA and lead instead to the formation of CoO_x clusters. These clusters reduce at lower temperatures than exchanged Co^{2+} species bound within inorganic aluminosilicates and are expected to exhibit redox properties more conducive to catalytic turnovers in oxidation reactions than bound isolated cations (Section 3.3.2).

3.3. Consequences of encapsulation for CoO_x reactivity and diffusional effects on reaction rates as evidence for encapsulation

The size and dispersity of CoO_x clusters in CoNaLTA (Section 3.2.2) are consistent with encapsulation within zeolite crystals because of the absence of large structures, their thermal stability, and their unlikely dispersion on the limited external areas of LTA

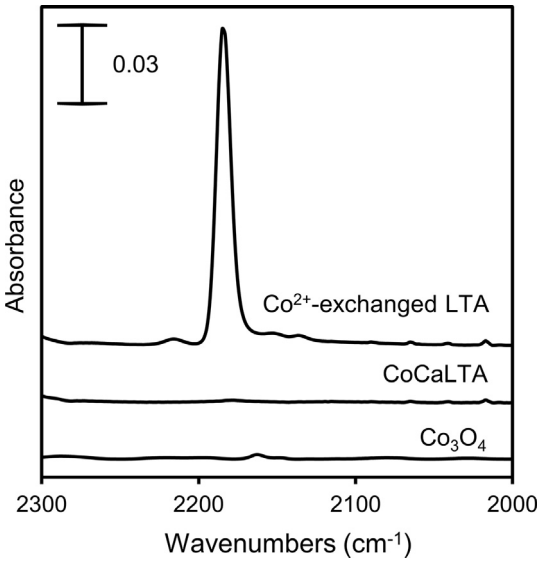

Fig. 6. Infrared spectra of CO adsorbed on Co_3O_4, CoCaLTA, and Co^{2+}-exchanged LTA samples at 313 K (1.0 kPa CO, 99.0 kPa He) after treatment in flowing He (0.7 cm^3 g^{-1} s^{-1}) at 473 K for 1 h.

crystals. These CoO_x particles are highly dispersed (1.4–1.6 nm diameter), thermally stable (in 873 K air treatment, 3 h), narrowly distributed in size (DI 1.03–1.07), and uniformly dispersed throughout zeolite crystals (Fig. 3). These properties would be atypical for extracrystalline structures, but reflect instead confinement effects that impose thermodynamic and kinetic obstacles to coalescence and sintering [13,14,24]. Their catalytic properties, however, provide the motivation for their synthesis, and the ability of only certain molecules to contact active sites, based on their size and diffusion properties, remain the ultimate arbiter of the selectivity of the synthetic protocols in enforcing encapsulation.

Here, we provide evidence for CoO_x encapsulation from ethanol (EtOH) oxidation reaction rates on Co-LTA samples with varying aperture widths, imposed by the presence of K^+, Na^+, or Ca^{2+} cations (Section 2.2.2). Turnover rates that increase as the apertures are made larger to allow more facile access to intracrystalline regions and faster reactant diffusion would then serve as evidence for the presence of active sites within constrained environments, accessible only via such diffusive processes. These effects of cation substitution, when interpreted in terms of appropriate kinetic-transport formalisms, also lead to precise estimates for the encapsulation selectivity, defined here as the fraction of active CoO_x surface area residing within LTA crystals in each sample.

3.3.1. Ethanol oxidation rates on cobalt-LTA catalysts as a probe for deducing encapsulation selectivity

Molecules, whether reactants or poisons, cannot contact active sites and react unless their size allows intracrystalline diffusion in the time scale of catalytic turnover rates. The intracrystalline voids can also preferentially stabilize transition states based on their size and fit within such voids [13,14,19,24]. Here, we exploit the size-selective properties of LTA zeolites by measuring ethanol (EtOH, 0.40 nm kinetic diameter [24]) oxidation rates on CoNaLTA samples exchanged with K^+ or Ca^{2+} cations (to form CoKLTA, CoNaLTA, $CoCa_{0.5}Na_{0.5}$LTA, or CoCaLTA; Section 2.2.2) in order to vary their diffusion properties and to estimate the fraction of the CoO_x surface area that resides within zeolite crystallites.

LTA zeolites with these different cations contain apertures of different size (i.e., KLTA: 0.3 nm, NaLTA: 0.4 nm, CaLTA: 0.5 nm; Section 2.2.2) because they differ in the number and size of the exchanged species [23]. These apertures determine the approximate size of molecules that can traverse such openings and access intracrystalline active sites [48]; their unequivocal interpretation as a precise pore dimension is precluded by temperature-dependent framework and molecular distortions [48], but the trends of diffusivity with the various cations is clear and well-established [23]. The identity of the exchanged cation would affect EtOH oxidation rates only when CoO_x structures predominantly reside within LTA crystals, because of concomitant effects on EtOH concentration gradients, and specifically, rates would increase as apertures become larger (in the order CoKLTA, CoNaLTA, $CoCa_{0.5}Na_{0.5}$LTA, CoCaLTA).

EtOH oxidation rates were measured at 423–523 K on these samples at 1 and 3 wt.% Co loadings (Section 2.3.7). Turnover rates are defined here as the molar rate of EtOH conversion per surface Co atom (estimated from the metal loading, $\langle d_{TEM} \rangle$ and the surface area; density of Co atoms in Co_3O_4; Section 2.3.7); these rates are shown in Fig. 7 as a function of reciprocal temperature. Acetaldehyde was the only detectable product for each sample. Rates increased exponentially with temperature (appearing linear on the Arrhenius plot) on all samples. EtOH turnover rates are higher on LTA zeolites with larger apertures at all temperatures, consistent with weaker EtOH concentration gradients as its diffusion becomes more facile. For instance, turnover rates on CoCaLTA were about 40-fold higher than on CoKLTA, indicative of severe constraints in accessing intracrystalline CoO_x active structures in

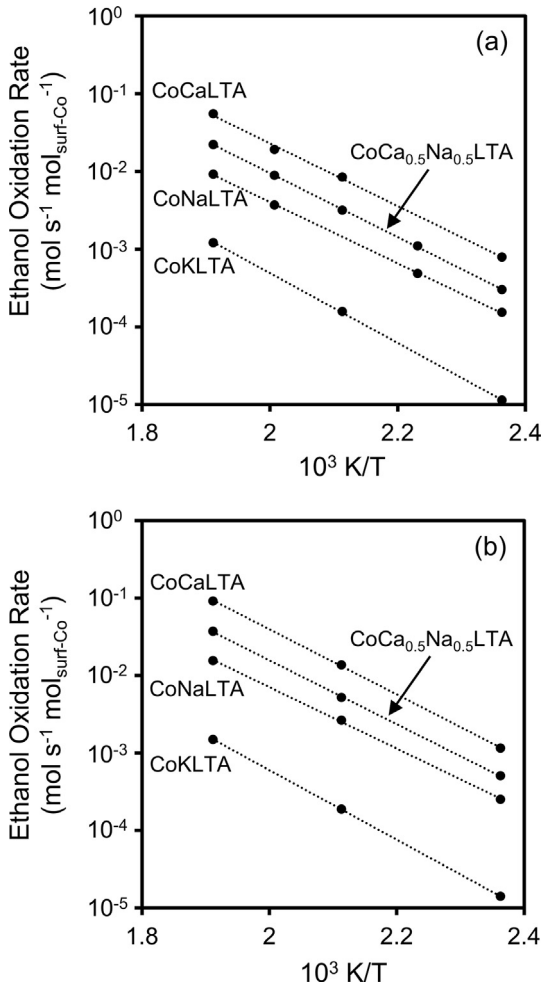

Fig. 7. Ethanol oxidation turnover rates (per surface Co atom) on CoKLTA, CoNaLTA, $CoCa_{0.5}Na_{0.5}$LTA, and CoCaLTA samples with (a) 3 wt.% and (b) 1 wt.% Co loading at 423–523 K (9 kPa O_2, 4 kPa ethanol, 88 kPa He). Samples were treated in 20% O_2/He (1.67 $cm^3\ g^{-1}\ s^{-1}$) at 573 K for 1 h before rate measurements.

CoKLTA. Turnover rates on $CoCa_{0.5}Na_{0.5}$LTA were intermediate between those on CoNaLTA and CoCaLTA, reflecting the faster diffusion allowed by the partial replacement of two Na^+ for each Ca^{2+}. These results are consistent with previous studies of EtOH oxidation rates on LTA-encapsulated Au clusters, which showed that the narrow LTA apertures lead to diffusional effects on EtOH oxidation rates [13].

The kinetic diameter of ethanol (0.40 nm) [14] is larger than the effective pore diameter of KLTA (0.3 nm) [23], suggesting that turnover rates measured on CoKLTA samples arise predominantly from reaction events occurring on extracrystalline CoO_x surfaces. The kinetic diameter is defined as the effective size of a molecule, taken from its cross section for scattering in gaseous collisions using spherical constructs [49]. Therefore, it neglects distinct orientations, molecular flexibility, and vibrational motions that determine which molecules can traverse the pore space, thus allowing the possible diffusion of some EtOH even into CoKLTA crystals.

The intrinsic reactivity of CoO_x surfaces depends on cluster size for many oxide-catalyzed reactions [1,3–5]. The reducibility of active Co^{3+} species involved in oxidation reactions [3,50] decreases as the CoO_x clusters become smaller because of more intimate interactions with less reducible supports [5] and higher LUMO energies [34], leading to the ubiquitous lower reactivity of smaller oxide domains. Alkanol oxidation reactions in particular proceed on cobalt oxide surfaces via redox cycles involving the reduction

of lattice cobalt cations and their re-oxidation by O_2 [50]. Consequently, alkanols such as methanol [50] and ethanol exhibit higher intrinsic oxidation rates on the more reducible surfaces of large CoO_x particles. Higher Co contents lead to higher active surface areas for clusters of a given size; as a result, they can create stronger concentration gradients within crystallites that restrict diffusion. In our studies, cluster sizes were nearly identical at the two Co loadings used on all samples (Section 3.2.2; CoKLTA, CoNaLTA, $CoCa_{0.5}Na_{0.5}$LTA, CoCaLTA; Fig. 3); thus, their different EtOH oxidation rates do not reflect cluster size effects on reactivity. Lower Co loadings (1 wt.%), however, gave higher turnover rates at all temperatures than samples with higher Co content (3 wt.%; Fig. 7), indicative of a greater kinetic load in 3 wt.% samples that causes more severe reactant depletion within LTA crystallites. These diffusion constraints on reactivity, taken together with the strong effects of the LTA charge balancing cation on measured rates (Fig. 7), confirm the predominant presence of CoO_x surfaces within LTA crystals that restrict EtOH access to active sites.

A more quantitative assessment of encapsulation selectivity can be derived by comparing EtOH oxidation rates on the two samples with the most different diffusional access ($r_{CoCaLTA}$ and r_{CoKLTA}). We define the CoO_x encapsulation selectivity (F) as:

$$F = 1 - \frac{r_{CoKLTA}}{r_{CoCaLTA}} \quad (3)$$

Its value becomes unity for active CoO_x surfaces that reside exclusively within LTA crystals. F increases with the extent of encapsulation, because $r_{CoCaLTA}$ accounts for the combined contributions of external and intracrystalline CoO_x, while r_{CoKLTA} mostly reflects the reactivity of those CoO_x surfaces fully accessible at KLTA external surfaces. F values would precisely account for the fraction of CoO_x surfaces within LTA only in the limiting case where r_{CoKLTA} values solely reflect external CoO_x surfaces and $r_{CoCaLTA}$ values reflect all surfaces, including those within crystals, when all surfaces are accessible to EtOH without diffusional hurdles. As a result, the F values defined as Eq. (3) are smaller than, and thus represent a lower limit to, the actual selectivity of encapsulation, because intracrystalline clusters within CoKLTA may contribute to some extent to the measured rates, while concentration gradients are likely to be present even within CoCaLTA.

These lower bounds for encapsulation selectivities are 0.97–0.99 for EtOH oxidation between 423 and 523 K and both 1 and 3 wt.% Co samples, indicating that >97% of active CoO_x surfaces reside within the protected environment of LTA crystals. These excellent high encapsulation selectivities are consistent with TEM results (Section 3.2.2), which appear to show CoO_x clusters that are uniformly distributed throughout LTA crystals, much smaller than plausible for unconfined particles at external LTA surfaces, and resistant to coalescence during thermal treatments. The selective encapsulation achieved and demonstrated here serves as the arbiter of success for the synthesis protocols that sought to confine clusters for specific catalytic benefits.

3.3.2. Comparison of CO and NO oxidation rates on CoNaLTA, CoCaLTA, Co^{2+}-exchanged LTA, and Co/SiO_2 samples

CO and NO oxidation rates were measured and evaluated to compare the catalytic properties of encapsulated cobalt oxide clusters with exchanged and unconfined Co species. CO oxidation rates, detectable on CoNaLTA (3 wt.% Co; $\langle d_{TEM}\rangle$ = 1.6 nm; DI: 1.06), CoCaLTA (3 wt.% Co; $\langle d_{TEM}\rangle$ = 1.6 nm; DI: 1.06), and Co/SiO_2 (30 wt.% Co; $\langle d_{TEM}\rangle$ = 21.0 nm; DI: 1.65), are shown in Fig. 8 as a function of temperature (473–543 K) in the form of an Arrhenius plot; CO_2 formation was not detectable on Co^{2+}-exchanged LTA (3 wt.% Co).

Measured CO oxidation rates gave linear trends in Fig. 8, as expected from CO oxidation rates limited by activated diffusion or chemical reactivity. CO oxidation on CoO_x surfaces proceeds via Mars-van Krevelen redox-cycles, limited by the reduction part, in which lattice O-atoms are removed to form vacancies via reaction with CO and the concurrent reduction of Co^{3+} cations [39,51]. Higher turnover rates have been reported on oxide surfaces with higher Co^{3+} concentrations (from X-ray photoelectron spectra, measured before reaction) [39,52]. Co^{2+}-exchanged LTA does not lead to detectable CO oxidation rates, even though infrared spectra show that CO can access intracrystalline Co^{2+} cations (Section 3.2.5), a consequence of the stable oxidation state of the prevalent Co^{2+} exchanged cations and consistent with the divalent and unreducible character of such exchanged species evident in reduction studies (Section 3.2.4). CoCaLTA, CoNaLTA, and Co/SiO_2 samples, in contrast, catalyze CO oxidation at detectable rates, indicating that Co_3O_4 species able to undergo redox cycles are present in these samples, as also shown by reduction rate data (Section 3.2.4).

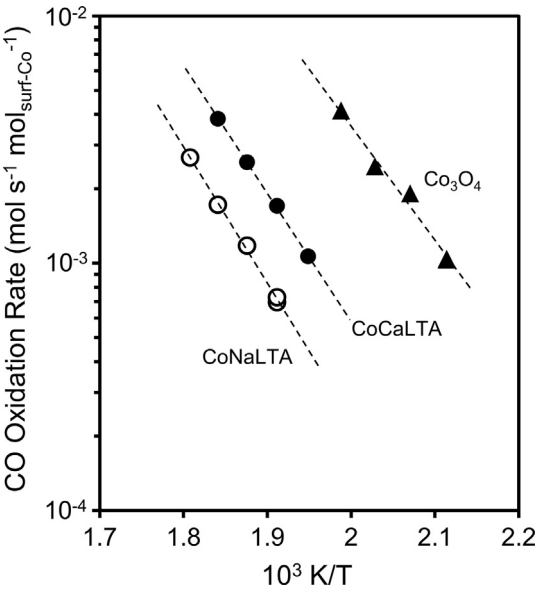

Fig. 8. CO oxidation turnover rates on CoCaLTA (●; 3 wt.% Co; $\langle d_{TEM}\rangle$ = 1.6 nm), CoNaLTA (○; 3 wt.% Co; $\langle d_{TEM}\rangle$ = 1.6 nm), and Co/SiO_2 (▲; 30 wt.% Co; $\langle d_{TEM}\rangle$ = 21 nm) samples at 473–543 K (1 kPa CO, 10 kPa O_2, 90 kPa He; 8.3 $cm^3\ g^{-1}\ s^{-1}$). Turnover rates are defined as the molar CO conversion rates per surface Co atom. Samples were treated in 20% O_2/He (8.3 $cm^3\ g^{-1}\ s^{-1}$) at 573 K for 1 h before rate measurements.

Turnover rates were twofold higher on CoCaLTA than on CoNaLTA at all temperatures, in spite of their similar Co content and oxide cluster size (Fig. 3), a reflection of the weaker diffusional constraints in CaLTA crystallites. Rates were even higher on Co/SiO_2, for which a given turnover rate (0.002 s^{-1}) required a much lower temperature than on CoCaLTA (490 K vs. 530 K), as a result of the combined effects of residual concentration gradients in CoCaLTA and the larger and more reactive clusters prevalent in Co/SiO_2 (21.0 vs. 1.6 nm).

Similar trends were observed for NO oxidation rates measured as a function of temperature on CoCaLTA, Co^{2+}-exchanged LTA, and Co/SiO_2 samples (Section 2.3.8) to determine the temperatures required to reach a given turnover rate. NO oxidation on Co_3O_4 surfaces involves kinetically-relevant O_2 chemisorption on O-vacancies and fast subsequent steps leading to O_2 dissociation and NO-NO_2 interconversion [53]. Turnover rates are much lower on smaller clusters, because of the less reducible nature and lower vacancy coverages characteristic of smaller clusters, which delocalize electrons much less effectively than larger domains [53]. NO conversion rates were not detectable on Co^{2+}-exchanged LTA

(<0.05%) over the temperature range 473–633 K, indicative of the substantial absence of Co_3O_4 clusters in these samples and their consequent inability to undergo Co^{3+}/Co^{2+} redox cycles. The temperatures required to reach a given turnover rate (0.002 s^{-1}, 0.003 s^{-1}, 0.004 s^{-1}) were higher on CoCaLTA (600 K, 620 K, 630 K) than Co/SiO_2 (550 K, 560 K, 565 K), an expected consequence of the significantly smaller Co_3O_4 clusters in CoCaLTA (1.6 nm) relative to Co/SiO_2 (21.0 nm), combined with the likely presence of NO and O_2 concentration gradients within CaLTA crystals.

These data show that Co_3O_4 nanoparticles within LTA crystals are less active than larger unconfined particles for CO and NO oxidation, as a consequence of the lower intrinsic reactivity of smaller clusters and of diffusional hurdles imposed by the LTA framework. Such small and stable encapsulated oxides make more efficient use of metal atoms, by exposing larger fractions of them at surfaces, and retain much higher dispersions through unique stabilization conferred by confinement. They also exploit molecular sieving effects that allow the preferential ingress and egress of specific reactant or product molecules, and can protect Co_3O_4 surfaces from deactivation by large poisons, such as sulfur compounds, which would titrate unconfined cobalt oxide clusters [54]. The inert character of exchanged Co^{2+} cations precludes the use of Co^{2+} exchange as a route to active catalysts that exploit the sieving properties of zeolite frameworks.

The synthesis protocols described here lead to Co oxide nanoparticles that are small and stable, as well as uniform in size and in their placement within zeolite crystals (Section 3.2). They reside predominantly within the protected environment of LTA frameworks (Section 3.3.1) and, in contrast with exchanged cations, catalyze oxidations of EtOH, CO, and NO (Section 3.3). The materials prepared make efficient conversion of Co precursors to active species through their selective retention within the crystals formed and by preventing their exchange onto LTA or the formation of Co aluminosilicates (Section 3.2.5). In doing so, these methods and the mechanistic inquiries that led to their optimization provide a much more general route for the preparation of zeolite-encapsulated base metal catalysts via hydrothermal assembly than the specific examples at hand may seem to indicate (Section 3.1); such examples are meant to provide the basis for the general platform that we proposed through the results presented here.

4. Conclusion

A synthesis procedure was developed for the selective encapsulation of cobalt oxide clusters within LTA zeolite crystals using a hydrothermal synthesis protocol with ligated Co^{2+} precursors. The method offers an alternative to more common encapsulation strategies that rely on reductive treatments of ion-exchanged metal cations, which are difficult or impossible to implement for Co because of the poor reducibility of zeolite-exchanged base metal cations. Metal encapsulation is conferred by introducing cobalt coordination complexes into zeolite synthesis gels and subsequently assembling the zeolite framework around such metal complexes. The Co^{2+} cations are stabilized by bifunctional ligands, which include a bidentate amine functionality to stabilize the cation against precipitation in the alkaline gels, and alkoxysilane groups, which can form siloxane bridges with nucleating zeolite precursors to promote metal uptake into the crystallized zeolites. Oxidative treatment of the ligated cobalt species occluded in the zeolite pores removes ligand residues and forms cobalt oxide clusters that are highly dispersed (1.4–1.6 nm), uniformly distributed in size (dispersity index 1.03–1.07), and thermally stable. The high dispersion and sinter-stability of such clusters results from their containment within the zeolite crystals, which impose thermodynamic barriers that limit the size to which the oxide clusters can grow. Temperature programmed reduction and infrared spectroscopy experiments indicate that the synthesis and post-synthetic treatment procedures preclude the formation of exchanged Co^{2+} or Co aluminosilicates; instead, the cobalt species selectively form Co_3O_4 clusters suitable for use in reactions catalyzed by cobalt oxides. Such clusters overwhelmingly reside within zeolite crystals, as confirmed with ethanol oxidation reactivity studies conducted on LTA samples of variable effective aperture diameters. The encapsulated Co_3O_4 clusters, in contrast with exchanged Co^{2+} cations, are also active for CO and NO oxidation. This work illustrates a synthesis strategy that can be employed to prepare cobalt oxide clusters that are well-defined and small in size and thermally stable, allowing systematic studies of cobalt oxide catalysts under conditions that favor particle sintering. Studies and applications of these materials can further exploit the molecular sieving and transition state selectivity conferred by the microporous voids and cavities of zeolites. We predict that the synthetic route used here can be more broadly applied to other zeolites and base metal species (e.g. Ni, Fe, Cu), for which existing cluster encapsulation techniques are limited or unavailable.

Notes

The authors declare the following competing financial interest (s): (1) The funding for the research came from Chevron Energy Technology Co. and (2) Stacey I. Zones is an employee of this company and, more generally, is also a stockholder in Chevron Corp.

Acknowledgements

We gratefully acknowledge the Chevron Energy Technology Co for their generous financial support of this research, as well as ancillary support provided for TO by an ARCS foundation fellowship and a National Science Foundation fellowship. We also thank Dr. Reena Zalpuri (Electron Microscope Lab) and Dr. Antonio DiPasquale (X-Ray Facility) for support with TEM and XRD instrumentation, respectively.

Appendix A. Supplementary material

X-Ray diffraction patterns of as-synthesized and air treated CoNaLTA samples, ultraviolet-visible spectra of supernatant solutions remaining after CoNaLTA synthesis, micropore volume of 3 wt.% CoNaLTA and CoCaLTA, temperature programmed oxidation profiles of as-synthesized 1 wt.% CoNaLTA, DR UV-vis analysis of CoNaLTA and Co^{2+}-exchanged LTA samples, electron micrographs of cobalt oxide clusters in 1 wt.% CoNaLTA after thermal treatment, IR spectra of adsorbed CO, and XRD patterns of CoCaLTA after 1020 K air or H_2 treatment. Supplementary data associated with this article can be found, in the online version, at https://doi.org/10.1016/j.jcat.2017.10.017.

References

[1] X. Xie, W. Shen, Nanoscale 1 (2009) 50–60.
[2] K. El Kabouss, M. Kacimi, M. Ziyad, S. Ammar, A. Ensuque, J.Y. Piquemal, F. Bozon-Verduraz, J. Mater. Chem. 16 (2006) 2453–2463.
[3] F. Wyrwalski, J.M. Giraudon, J.F. Lamonier, Catal. Lett. 137 (2010) 141–149.
[4] J. Zhu, K. Kailasam, A. Fischer, A. Thomas, ACS Catal. 1 (2011) 342–347.
[5] H. Jahangiri, J. Bennett, P. Mahjoubi, K. Wilson, S. Gu, Catal, Sci. Technol. 4 (2014) 2210–2229.
[6] T.O. Eschemann, J.H. Bitter, K.P. de Jong, Catal. Today 228 (2014) 89–95.
[7] J.-C. Kim, S. Lee, K. Cho, K. Na, C. Lee, R. Ryoo, ACS Catal. 4 (2014) 3919–3927.
[8] B.B. Lakshmi, C.J. Patrissi, C.R. Martin, Chem. Mater. 9 (1997) 2544–2550.
[9] Z. Meng, B. Liu, J. Zheng, Q. Sheng, H. Zhang, Microchim. Acta 175 (2011) 251–257.
[10] M. Salavati-Niasari, A. Khansari, F. Davar, Inorg. Chim. Acta 362 (2009) 4937–4942.

[11] M. Ghosh, E.V. Sampathkumaran, C.N.R. Rao, Chem. Mater. 17 (2005) 2348–2352.
[12] G.A. Ferguson, C. Yin, G. Kwon, E.C. Tyo, S. Lee, J.P. Greeley, P. Zapol, B. Lee, S. Seifert, R.E. Winans, S. Vajda, L.A. Curtiss, J. Phys. Chem. C 116 (2012) 24027–24034.
[13] T. Otto, S.I. Zones, E. Iglesia, J. Catal. 339 (2016) 195–208.
[14] T. Otto, J.M. Ramallo-López, L.J. Giovanetti, F.G. Requejo, S.I. Zones, E. Iglesia, J. Catal. 342 (2016) 125–137.
[15] Z. Wu, S. Goel, M. Choi, E. Iglesia, J. Catal. 311 (2014) 458–468.
[16] J.D. Rimer, M. Kumar, R. Li, A.I. Lupulescu, M.D. Oleksiak, Catal. Sci. Tech. 4 (2014) 3762–3771.
[17] E. Asedegbega-Nieto, Eva Díaz, A. Vega, S. Ordóñez, Catal. Today 157 (2010) 425–431.
[18] A. Borqschulte, E. Callini, N. Stadie, Y. Arroyo, M.D. Rossell, R. Erni, H. Geerlings, A. Züttel, D. Ferri, Catal. Sci. Technol. 5 (2015) 4613–4621.
[19] P.B. Weisz, V.J. Frilette, R.W. Maatman, E.B. Mower, J. Catal. 1 (1962) 307–312.
[20] G. Bergeret, P. Gallezot, in: Handbook of Heterogeneous Catalysis, Wiley-VHC, Weinheim, Germany, 2008, pp. 738–765.
[21] P. Paoletti, Pure Appl. Chem. 56 (1984) 491–522.
[22] IZA Synthesis Commission, Synthesis Recipes in the 2nd Edition of Verified Syntheses of Zeolitic Materials, http://www.iza-online.org/synthesis (accessed Feb 22, 2017).
[23] O. Cheung, N. Hedin, RSC Adv. 4 (2014) 14480–14494.
[24] M. Choi, Z. Wu, E. Iglesia, J. Am. Chem. Soc. 132 (2010) 9129–9137.
[25] A.M. Garcia Rodriguez, A. Garcia de Torres, J.M. Cano Pavon, C. Bosch Ojeda, Talanta 47 (1998) 463–470.
[26] B. Małecka, A. Łącz, E. Drożdż, A. Małecki, J. Therm. Anal. Calorim. 119 (2015) 1053–1061.
[27] I.S. Kotousova, S.M. Polyakov, Kristallografiya 17 (1972) 661–663.
[28] R.D. Shannon, Acta Crystallogr. A 32 (1976) 751–767.
[29] T.J. Smith, J. Mol. Graphics 13 (1995) 122–125.
[30] W.V. Knowles, M.O. Nutt, M.S. Wong, in: J.R. Regalbuto (Ed.), Catalyst Preparation: Science and Engineering, CRC Press, Inc., Boca Raton, FL, 2007, pp. 258–259.
[31] A. Kogelbauer, J.C. Weber, J.G. Goodwin Jr., Catal. Lett. 34 (1995) 259–267.
[32] L.J. Garces, B. Hincapie, R. Zerger, S.L. Suib, Phys. Chem. C 119 (2015) 5484–5490.
[33] G. Jacobs, T.K. Das, Y. Zhang, J. Li, G. Racoillet, B.H. Davis, Appl. Catal. A 233 (2002) 263–281.
[34] D.G. Barton, M. Shtein, R.D. Wilson, S.L. Soled, E. Iglesia, J. Phys. Chem. B 103 (1999) 630–640.
[35] Y. Okamoto, K. Nagata, T. Adachi, T. Imanaka, K. Inamura, T. Takyu, J. Phys. Chem. 95 (1991) 310–319.
[36] S. Lim, D. Ciuparu, Y. Chen, L. Pfefferle, G.L. Haller, J. Phys. Chem. B 108 (2004) 20095–20101.
[37] D.J. Moodley, A.M. Saib, J. van de Loosdrecht, C.A. Welker-Nieuwoudt, B.H. Sigwebela, J.W. Niemantsverdriet, Catal. Today 171 (2011) 192–200.
[38] S. Bhatia, Zeolite Catalysis: Principles and Applications, CRC Press Inc, Boca Raton, FL, 1990, p. 10.
[39] V. Iablokov, R. Barbosa, G. Pollefeyt, I. Van Driessche, S. Chenakin, N. Kruse, ACS Catal. 5 (2015) 5714–5718.
[40] R. Dieckmann, Z. Phys. Chem. 107 (1977) 189–210.
[41] C.L. Angell, P.C. Schaffer, J. Phys. Chem. 70 (1966) 1413–1417.
[42] V. Rakić, V. Dondur, R. Hercigonja, J. Serb. Chem. Soc. 68 (2003) 409–416.
[43] M. Moskovits, J.E. Hülse, Surf. Sci. 78 (1978) 397–418.
[44] H.K. Lin, C.B. Wang, H.C. Chiu, S.H. Chien, Catal. Lett. 86 (2003) 63–68.
[45] A.Y. Khodakov, J. Lynch, D. Bazin, B. Rebours, N. Zanier, B. Moisson, P. Chaumette, J. Catal. 168 (1997) 16–25.
[46] G. Busca, V. Lorenzelli, V.S. Escribano, R. Guidetti, J. Catal. 131 (1991) 167–177.
[47] V. Subramanian, V.L. Zholobenko, K. Cheng, C. Lancelot, S. Heyte, J. Thuriot, S. Paul, V.V. Ordomsky, A.Y. Khodakov, ChemCatChem 8 (2016) 380–389.
[48] R.F. Lobo, in: S.M. Auerbach, K.A. Carrado, P.K. Dutta (Eds.), Handbook of Zeolite Science and Technology, Marcel Dekker Inc., New York, New York, USA, 2003, pp. 71–72.
[49] N. Mehio, S. Dai, D. Jiang, J. Phys. Chem. A 118 (2014) 1150–1154.
[50] M.M. Natile, A. Glisenti, Chem. Mater. 14 (2002) 3090–3099.
[51] P. Broqvist, I. Panas, H. Persson, J. Catal. 210 (2002) 198–206.
[52] Y. Xie, F. Dong, S. Heinbuch, J.J. Rocca, E.R. Bernstein, Phys. Chem. Chem. Phys. 12 (2010) 947–959.
[53] B.M. Weiss, N. Artioli, E. Iglesia, ChemCatChem 4 (2012) 1397–1404.
[54] Y. Huang, D. Gao, Z. Tong, J. Zhang, H. Luo, J. Nat. Gas Chem. 18 (2009) 421–428.